Journal of Power Sources 201 (2012) 179–183

Contents lists available at SciVerse ScienceDirect

Journal of Power Sources

journal homepage: www.elsevier.com/locate/jpowsour

Short communication

Ultrasound-assisted polyol synthesis and electrocatalytic characterization of Pd_xCo alloy and core–shell nanoparticles

Ji-Hoon Jang[a], Chanho Pak[b], Young-Uk Kwon[a,*]

[a] Department of Chemistry, BK-21 School of Chemical Materials Sciences, SAINT/HINT, Sungkyunkwan University, Suwon 440-746, Republic of Korea
[b] Samsung Advanced Institute of Technology, Yongin 446-712, Republic of Korea

ARTICLE INFO

Article history:
Received 1 August 2011
Received in revised form 17 October 2011
Accepted 26 October 2011
Available online 20 November 2011

Keywords:
Nanomaterials
Ultrasound reaction
Polymer electrolyte membrane fuel cells
Oxygen reduction reaction
Electrocatalysis

ABSTRACT

Carbon supported Co–Pd nanocomposites with two different surface compositions and various Co/Pd ratios have been synthesized by an ultrasound-assisted polyol process. Sonochemical treatment of palladium acetylacetonate and cobalt acetylacetonate in ethylene glycol in the presence of a carbon support without added surfactant, pH adjuster, or stabilizer has produced 4–7 nm Pd_xCo nanoparticles dispersed on the carbon support. The absence of additives has led to purer nanoparticles than produced by conventional wet methods. The structures of nanoparticles – pure Pd, Co–Pd alloy, and core–shell – have been characterized by XRD, TEM, EELS, and STEM. Electrocatalysis of oxygen reduction reactions of the materials have been measured using rotating disk electrodes and are compared with pure Pd/C and commercial Pt/C. The Co–Pd mixed phase samples show higher specific activity than pure Pd/C and comparable performance to commercial Pt/C. The Pd_4Co core–shell structure shows significantly enhanced catalytic activity.

1. Introduction

Bimetallic alloy or core–shell nanoparticles (NPs) that contain transition and noble metals have potential uses in various fields, such as electrocatalysis in fuel cells [1–7] and magnetic materials [8–10]. They are characterized by the structural strain arising from the different sizes of the constituent atoms, which features afford structural diversity and the possibility of tunable properties. In core–shell NPs, the strain at the interface between the core and the shell can be very large, strongly influencing the NPs' properties [1,4,7].

Each of the various techniques reported for the preparation of bimetallic NPs [11–20] has its drawbacks. Multi-step processes for core–shell NPs involve lengthy preparation. Harsh reaction conditions with strong reducing reagents and the presence of surfactants or stabilizing polymers that control NPs' sizes and shapes can cause problems; Liu and Manthiram reported that they reduce catalytic activity [3].

Pd-based NPs, comprising such as Pd_4Co, have been studied with the aim to replace expensive Pt in electrodes [7,15,18]. Suo et al. synthesized Pd_xCo bimetallic NPs with only (1 1 1) surfaces that showed greatly enhanced electrocatalytic activity towards the oxygen reduction reaction (ORR) [7]. Lattice contraction, which reduced the energy of O_2 adsorption onto the catalyst surface, was important in improving ORR activity. The larger strain in core–shell NPs suggests their greater catalytic activity than alloyed NPs. This is supported by some theoretical studies. However, all works characterizing synthesized NPs have studied only one of the two types, with no direct experimental comparison between both of them.

Therefore, this work reports the synthesis and characterization of alloyed and core–shell Pd_4Co NPs on carbon supports (denoted as Pd_4Co/C(AL) and Pd_4Co/C(CS)). A novel ultrasound-assisted polyol process was developed for the syntheses. Ultrasound has been used to produce various NPs, including bimetallic NPs [21], however, its use in the synthesis of Pd–Co NPs or core–shell NPs has not been previously reported.

2. Experimental

2.1. Catalysts preparation

Pd_xCo nanoparticles on carbon supports were synthesized by an ultrasound-assisted polyol process with different surface structures – Co-rich cores and Pd-rich shells (CS) and Pd–Co alloys (AL) – and various ratios of Pd/Co (1/0, 1/0.125, 1/0.250, and 1/0.333). The synthetic method was modified to produce each structural type. CS NPs were synthesized by first dispersing cobalt acetylacetonate (Aldrich, $Co(acac)_2$) in ethylene glycol (Samchun Chemical, EG), prepurging it with Ar for 30 min, and irradiating the dispersion with a high-intensity ultrasonic probe (Sonic and

* Corresponding author. Tel.: +82 31 290 7070; fax: +82 31 290 7075.
E-mail address: ywkwon@skku.edu (Y.-U. Kwon).

0378-7753/$ – see front matter © 2011 Elsevier B.V. All rights reserved.
doi:10.1016/j.jpowsour.2011.10.139

Materials, VC-500, 30% amplitude, 20 kHz, with 13 mm solid probe) for 30 min under Ar to prepare cobalt seeds. Palladium acetylacetonate (Aldrich, $Pd(acac)_2$) and graphitic Ketjen black (GKB, support from SAIT) were subsequently added to the above mixture and irradiated continuously for 150 min. The resulting dark slurry was filtrated through a Nylon membrane (Whatman Int., Ltd.), repeatedly washed with ethanol, and dried under vacuum for 12 h at room temperature. AL NPs were produced similarly, except that $Pd(acac)_2$, $Co(acac)_2$, and GKB were added to the solutions simultaneously. The two sets of materials are denoted as $Pd_xCo/C(CS)$ and $Pd_xCo/C(AL)$, respectively.

2.2. Characterization

Samples were characterized by X-ray diffractometry (XRD, DC/Max 2000, Rigaku, CuKα (λ = 1.54056 Å)) and high-resolution transmission electron microscopy (HR-TEM, JEOL JEM-3011) operating at 300 kV. Elemental compositions were assessed by energy dispersive X-ray spectroscopy (EDS) in conjunction with field emission scanning electron microscopy (FE-SEM, JEOL JSM-7300F). Five different areas of each sample were analyzed to obtain averaged compositions. Individual NPs' elemental compositions were recorded by EDS attached on field emission transmission electron microscopy (FE-TEM, JEOL, JEM-2100F) with a ~1 nm probe under the scanning transmission electron microscope (STEM) mode. Electron energy loss spectroscopy (EELS) analysis was conducted using a ~0.13 nm probe under STEM mode in JEOL ARM200F Cs-corrected TEM.

2.3. Electrochemical analysis

Electrocatalytic behavior was assessed by an Ivium compactstat electrochemical analyzer (Ivium Technology) using a standard three-electrode electrochemical cell and a rotating disk electrode (RDE, Autolab). 3 mg electrocatalyst was dispersed in 1.5 g deionized water by sonication, 5 μL of which was dropped onto a working electrode (glassy carbon, d = 3 mm) and dried in air. 5 μL 0.05 wt% Nafion solution was covered on the working electrode for mechanical protection from the rotation of the RDE. A Pt mesh and a Ag/AgCl electrode were used as the counter and reference electrodes, respectively. The potential range shown in the figures was converted to be referenced to a reversible hydrogen electrode (RHE). To eliminate impurities and to obtain clearer results, the working electrode was repeatedly electrochemically cleaned before each measurement. Cyclic voltammograms (CV) were recorded in aqueous 0.1 M $HClO_4$ at a scan rate of 50 mV s^{-1}. Electrocatalytic surface areas (ESAs) of the electrocatalysts were obtained by calculating the areas of the hydrogen active regions in the CV curves; calibration was made against the 210 μC cm^{-2} of polycrystalline Pt and Pd. Electrocatalytic activity towards the ORR was measured by linear sweep voltammetry (LSV) in 30 min-O_2 saturated electrolyte (0.1 M $HClO_4$) at a scan rate of 5 mV s^{-1} and a rotation speed of 1600 rpm.

3. Results and discussion

3.1. Structural analysis

Syntheses were achieved by the ultrasound irradiation of ethylene glycol solutions of $Pd(acac)_2$ (acac = acetylacetonate) and $Co(acac)_2$ in the presence of carbon supports under Ar. $Pd_4Co/C(CS)$ was synthesized by reacting the Co reagent first to form Co seeds with subsequent addition of the Pd reagent under ultrasound irradiation. $Pd_4Co/C(AL)$ was synthesized with both Co and Pd reagents reacted simultaneously under ultrasound irradiation. The reaction conditions were otherwise the same in both cases. Pd NPs supported on carbon were also similarly prepared without the Co reagent. Ethylene glycol, which may have acted as a mild stabilizing agent, was the only additive used in these syntheses.

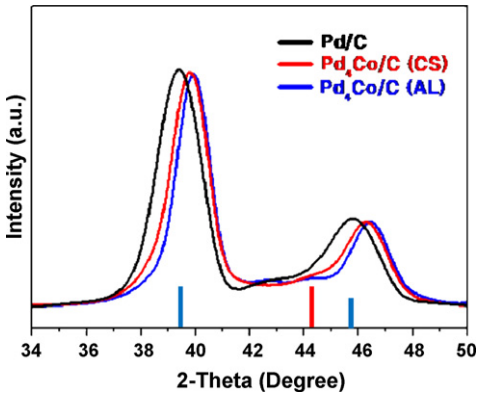

Fig. 1. XRD patterns of Pd/C, $Pd_4Co/C(CS)$, and $Pd_4Co/C(AL)$. Vertical red and blue lines indicate the diffraction peaks of Co (JCPDS, 15-0806) and Pd (JCPDS, 87-0641), respectively, both in face centered cubic structures. (For interpretation of the references to color in this figure legend, the reader is referred to the web version of the article.)

The two samples were shown to have identical compositions, within experimental error, by EDS/SEM carried out (Table S1). Macroscopic homogeneity of the electrocatalysts was confirmed by taking EDS measurement at five different areas (*ca.* 1 × 1 μm^2) of each sample. EDS/TEM was also used to verify the uniform compositions of individual NPs within the samples (Fig. S1).

Fig. 1 shows the XRD patterns of the materials. The Scherrer equation was used to calculate particles sizes: 6.1 nm for Pd/C, 6.3 nm for $Pd_4Co/C(CS)$, and 7.3 nm for $Pd_4Co/C(AL)$. The XRD patterns were indexed as face-centered cubic unit cells with a = 3.96 Å for Pd/C, a = 3.90 Å for $Pd_4Co/C(CS)$, and a = 3.88 Å for $Pd_4Co/C(AL)$. The lattice parameter of Pd/C was slightly larger than that of pure Pd (3.91 Å), indicating hydrogen absorption [22–25]. Pd_4Co showed smaller lattice parameters than Pd due to the incorporation of smaller Co atoms in the Pd lattice. The XRD patterns clearly show that, though small, $Pd_4Co/C(CS)$ has a larger lattice parameter than $Pd_4Co/C(AL)$. Since their compositions are identical, this is likely due to the differences of elemental distribution.

The Pd_4Co NPs were studied by TEM and EELS in conjunction with STEM. The low-magnification TEM image of Pd/C (Fig. S2(a)) shows its 5–8 nm spherical NPs well-dispersed on the carbon support. The magnified TEM image of a Pd NP (Fig. 2(a)) shows its polycrystalline nature with lattice fringes of (1 1 1) and (2 0 0) plains. Both Pd_4Co/C samples (Figs. S2(b) and (c)) comprised 5–8 nm NPs; triangular and spherical shaped NPs are mixed. All the triangular NPs appear to be single crystalline – the triangular faces were (1 1 1) facets (Figs. 2(b) and (d)). The spherical NPs show both single-crystallinity (Figs. 2(c) and (e)) and polycrystallinity (Fig. 2(f)). Therefore, both the Pd_4Co/C samples have larger fractions of (1 1 1) facets than Pd/C. The incorporation of Co appears to lower the surface energy of the NPs, inducing larger crystallites than in pure Pd. This does not necessarily imply different elemental compositions across differently shaped NPs: because the EDS spectra of differently shaped individual NPs showed similar compositions (Fig. S1). Also, the average lattice spacing of differently shaped NPs, taken over at least ten repeating units, are close to each other. We used EELS analysis to see the direct evidence for the core–shell structure of $Pd_4Co/C(CS)$. Although EELS signals are very weak because the energy losses are recorded, it has much higher spatial resolution than that of EDS. The core–shell structure of $Pd_4Co/C(CS)$ was confirmed by EELS measurements of the edges

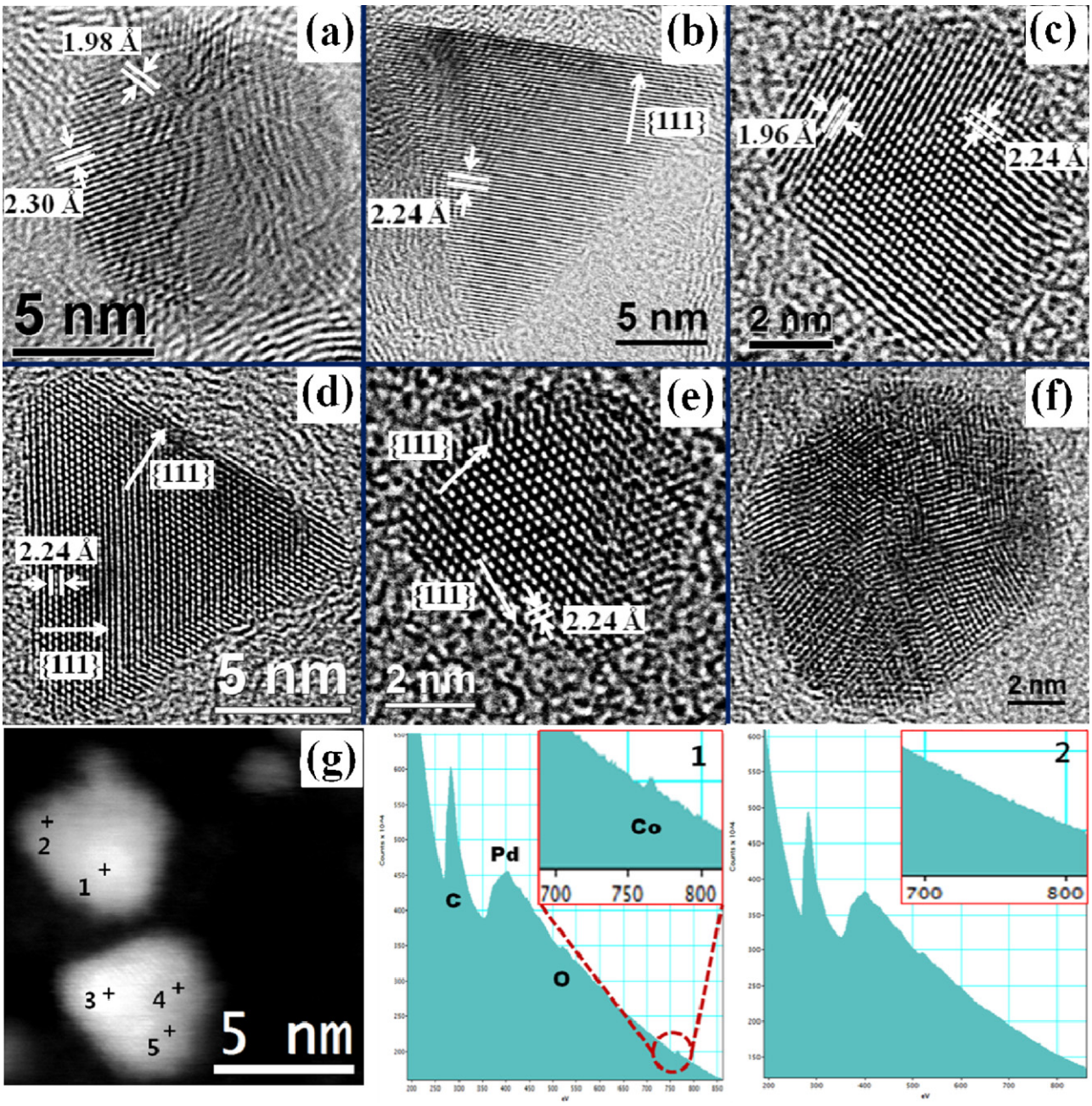

Fig. 2. HRTEM images of (a) Pd/C, (b) and (c) $Pd_4Co/C(CS)$, and (d)–(f) $Pd_4Co/C(AL)$. (g) STEM–EELS measurements of $Pd_4Co/C(CS)$. Other EELS spectra are shown in Fig. S3.

and centers of individual NPs (Fig. 2(g)) with the centers showed evidence of Co and Pd, the edges showed Pd only. Elemental mapping was not possible because the NPs were too small to remain still to record the data. Nevertheless, the EELS data (Figs. 2(g) and S3) are sufficient to confirm the core–shell structure of $Pd_4Co/C(CS)$.

3.2. Electrocatalysis studies

Electrochemical analyses were performed using a three-electrode cell in 0.1 M $HClO_4$ electrolyte. Each CV curve (Fig. 3(a)) of the synthesized NPs and commercial Pt/C (ETEK, 20 wt%) was recorded after the electrodes were electrochemically cleaned. Pt/C showed larger bilayer capacitance than the other materials due to the different carbon support. Commercial Pt/C comprised 2–3 nm Pt NPs supported on Vulcan carbon [26]. Electrocatalytic surface areas (ESAs, Fig. 3(c)) of the electrodes were estimated from the CV curves between 0.0 and 0.3 V with reference to the literature value of 210 $\mu C\,cm^{-2}$ for polycrystalline Pt. Pt/C showed the largest ESA of 49 $m^2\,g^{-1}$; Pd/C showed approximately half that, 24 $m^2\,g^{-1}$. The Pd_4Co/C samples showed ESAs between the two. The CV peaks of Pd_4Co/C in the hydrogen active region are different from that of Pd/C in their position and shape. Peaks at 0.05 V and 0.2 V for single crystal Pd electrodes have been reported to be associated with (1 1 1) and (1 0 0) facets of Pd, respectively [27]. These peaks in the CV of Pd/C are almost the same magnitude. The (1 1 1) facet dominates the CV curves of the two Pd_4Co/C samples, in accordance with the formation of single crystalline triangular NPs with (1 1 1) facets in these samples. $Pd_4Co/C(CS)$ showed a slightly larger ESA than $Pd_4Co/C(AL)$.

Linear sweep voltammograms (LSVs, Fig. 3(b)) were measured to assess electrocatalytic activity towards the ORR. The onset potentials were in the order: Pt/C > $Pd_4Co/C(CS)$ > $Pd_4Co/C(AL)$ > Pd/C. The

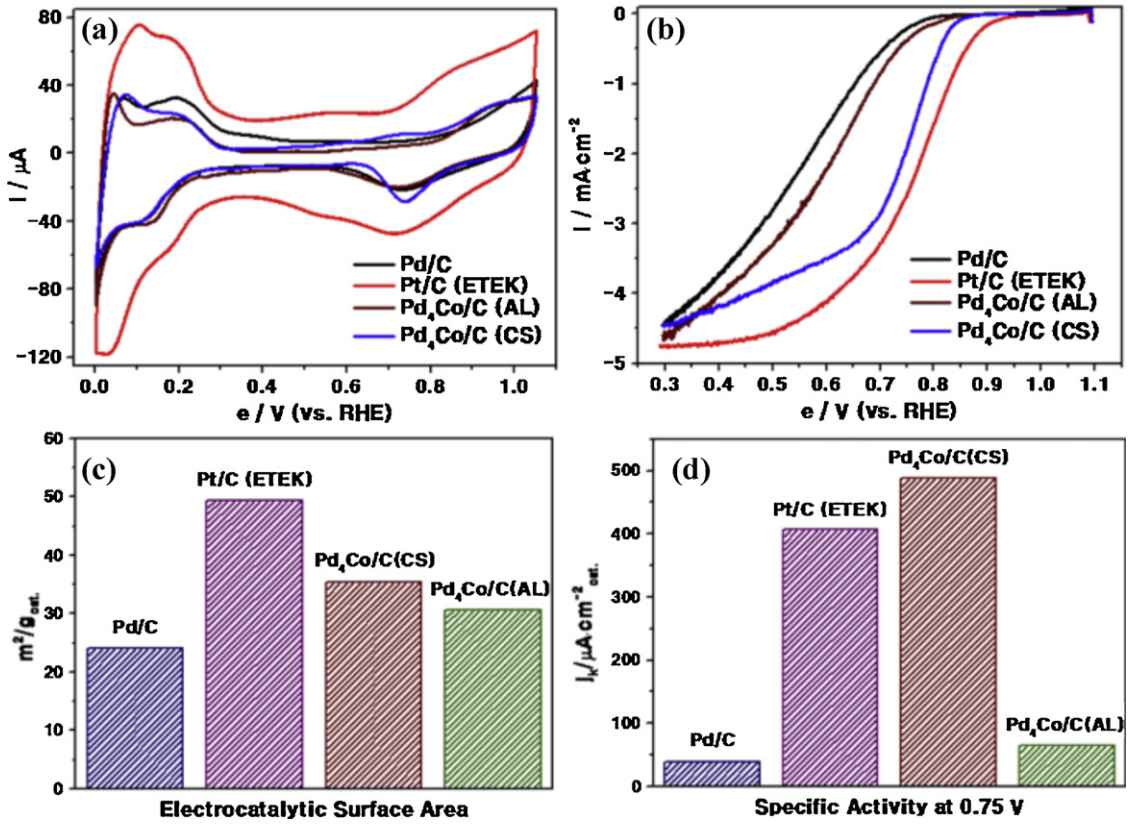

Fig. 3. Electrochemical analyses of Pd/C, Pt/C, and Pd_4Co/C (a) cyclic voltammograms (scan rate 50 mV s^{-1}, in 0.1 M $HClO_4$ under N_2). (b) Linear sweep voltammograms for ORR (scan rate 5 mV s^{-1}, in 0.1 M $HClO_4$ under O_2). (c) Electrodes' electrocatalytic surface areas, and (d) specific activities at 0.75 V (vs. RHE).

onset potential of $Pd_4Co/C(CS)$ was considerably higher than those of other Pd-containing materials and was close to that of Pt. The different catalytic activities of two Pd_4Co/C samples strongly indicate differences in the elemental distribution, attributable to differences in their syntheses. The high onset potential of $Pd_4Co/C(CS)$ agrees with theoretical predictions of core–shell NPs' properties. Partial electron donation from Co to Pd and compression of Pd–Pd bonds in the shells due to the Co cores are expected to raise the NPs' Fermi level and increase the onset potential [28,29].

To understand the electrocatalytic activities towards ORR, LSV results were normalized by the ESA values. From the normalized LSV data, specific activities at 0.75 V are compared in Fig. 3(d) (mass activities are compared in Fig. S4). The mass activity towards ORR of $Pd_4Co/C(CS)$ (173 mA mg^{-1}) is 86% of that of Pt/C (201 mA mg^{-1}). Although, the mass activity of $Pd_4Co/C(CS)$ is 28 mA mg^{-1} less than that of Pt/C, it is *ca.* 20 time larger than that of Pd/C (9 mA mg^{-1}). While mass activity is related to the capacity of the catalysts, specific activity is related to the reaction kinetics over a range of potentials. Specific activity is in the order: $Pd/C < Pd_4Co/C(AL) < Pt/C < Pd_4Co/C(CS)$. $Pd_4Co/C(CS)$ shows 12 time the specific activity of Pd/C and its specific activity is 80 μA cm^{-2} greater than that of Pt/C.

In addition to Pd_4Co/C, Pd_3Co/C, and Pd_8Co/C were also synthesized in both CS and AL structures. Their characterization and electrochemical analysis are summarized in Supporting Information (Table S1 and Figs. S5 and S6). Their general behavior is similar to that of Pd_4Co/C. However, they show lower catalytic activity towards ORR than the Pd_4Co/C samples. Suo et al. reported that a Pd/Co composition ratio of 11/1 showed the greatest catalytic activity towards the ORR [7]. To the contrary, the maximum activity was observed at a Pd/Co ratio of 4/1 in the present work. The discrepancy may be due to the use of multifaceted NPs here compared with the uniform (1 1 1) surfaces used by Suo et al.

4. Conclusion

An ultrasound-assisted synthesis of Pd_xCo bimetallic NPs supported on carbon was developed. It did not require any stabilizing agents to control the particles sizes. It allowed either alloy or core–shell NPs to be synthesized, enabling their direct comparison. The NPs were characterized by XRD, EDS, TEM, and EELS and were assessed for their electrochemical catalytic activity. Pd_4Co was close to the optimal composition for facilitating the ORR, with core–shell type NPs showing greater activity than alloyed NPs. The core–shell Pd_4Co NPs showed activity towards the ORR comparable to that of Pt. Further spectroscopic analyses of these particles, such as soft X-ray absorption spectroscopy, are underway to clarify their structural differences.

Acknowledgements

This work was supported by grants NRF-2010-0029698 (Priority Research Center Program) and NRF-2011-0006268 (Basic Science Research Program). We thank KBSI, CCRF and NNFC for the TEM, EELS, and EDX data.

Appendix A. Supplementary data

Supplementary data associated with this article can be found, in the online version, at doi:10.1016/j.jpowsour.2011.10.139.

References

[1] J. Greeley, M. Mavrikakis, Nat. Mater. 3 (2004) 810.
[2] S.J. Yoo, H.Y. Park, T.Y. Jeon, I.S. Park, Y.H. Cho, Y.E. Sung, Angew. Chem. Int. Ed. 47 (2008) 9307.
[3] H. Liu, A. Manthiram, Energy Environ. Sci. 2 (2009) 124.

[4] V. Stamenkovicĭ, T.J. Schmidt, P.N. Ross, N.M. Markovic, J. Phys. Chem. B 106 (2002) 11970.
[5] M. Shao, K. Sasaki, N.S. Marinkovic, L. Zhang, R.R. Adzic, Electrochem. Commun. 9 (2007) 2848.
[6] M. Shao, P. Liu, J. Zhang, R.R. Adzic, J. Phys. Chem. B 111 (2007) 6772.
[7] Y. Suo, L. Zhuang, J. Lu, Angew. Chem. Int. Ed. 46 (2007) 2862.
[8] J. Wang, K.P. Loh, Y.L. Zhong, M. Lin, J. Ding, Y.L. Foo, Chem. Mater. 19 (2007) 2566.
[9] X. Sun, Y. Huang, D.E. Nikles, Int. J. Nanotech. 1 (2004) 328.
[10] X.H. Xu, H.S. Wu, F. Wang, X.L. Li, Thin Solid Films 472 (2005) 222.
[11] S. Alayoglu, A.U. Nilekar, M. Mavrikakis, B. Eichhorn, Nat. Mater. 7 (2008) 333.
[12] I. Kazeminezhad, H.J. Blythe, W. Schwarzacher, Appl. Phys. Lett. 78 (2001) 1014.
[13] R. Tena-Zaera, A. Katty, S. Bastide, C. Lévy-Clément, Chem. Mater. 19 (2007) 1626.
[14] H. Lee, S.E. Habas, G.A. Somorjai, P. Yang, J. Am. Chem. Soc. 130 (2008) 5406.
[15] J.L. Fernandez, V. Raghuveer, A. Manthiram, A.J. Bard, J. Am. Chem. Soc. 127 (2005) 13100.
[16] R.F.C. Farrow, D. Weller, R.F. Marks, M.F. Toney, S. Hom, G.R. Harp, A. Cebollada, Appl. Phys. Lett. 69 (1996) 1166.
[17] J. Chen, B. Wiley, J. McLellan, Y. Xiong, Z.Y. Li, Y. Xia, Nano Lett. 5 (2005) 2058.
[18] F.H.B. Lima, J. Zhang, M.H. Shao, K. Sasaki, M.B. Vukmirovic, E.A. Ticianelli, R.R. Adzic, J. Solid State Electrochem. 12 (2008) 399.
[19] W. Chen, J. Kim, S. Sun, S. Chen, Phys. Chem. Chem. Phys. 8 (2006) 2779.
[20] H. Ye, R.M. Crooks, J. Am. Chem. Soc. 129 (2007) 3627.
[21] K.S. Suslick, Science 247 (1990) 1439.
[22] J.H. Jang, J. Kim, Y.H. Lee, Y.U. Kwon, Electrochim. Acta 55 (2009) 485.
[23] A.W. Hull, Phys. Rev. 17 (1921) 571.
[24] G. Bredig, R.Z. Allolio, Phys. Chem. Neue Folge 126 (1927) 41.
[25] T.B. Massalski, Binary Alloy Phase Diagrams, 2nd Ed., vol. 3, Codata, 1990, p. 1222.
[26] W. Vogel, J. Phys. Chem. C 112 (2008) 13475.
[27] N. Hoshi, K. Kida, M. Nakamura, M. Nakada, K. Osada, J. Phys. Chem. B 110 (2006) 12480.
[28] J.L. Fernandez, D. Walsh, A.J. Bard, J. Am. Chem. Soc. 127 (2005) 357.
[29] J.R. Kitchin, J.K. Norskov, M.A. Barteau, J.G. Chen, Phys. Rev. Lett. 93 (2004) 156801.